Accepted Manuscript

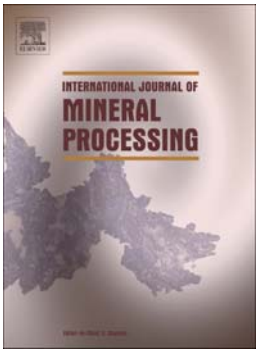

A review of the applications of the JK size-dependent breakage model part 3: Comminution equipment modelling

Fengnian Shi

PII: S0301-7516(16)30207-1
DOI: doi: 10.1016/j.minpro.2016.09.011
Reference: MINPRO 2961

To appear in: *International Journal of Mineral Processing*

Received date: 3 June 2016
Revised date: 22 September 2016
Accepted date: 29 September 2016

Please cite this article as: Shi, Fengnian, A review of the applications of the JK size-dependent breakage model part 3: Comminution equipment modelling, *International Journal of Mineral Processing* (2016), doi: 10.1016/j.minpro.2016.09.011

A review of the applications of the JK size-dependent breakage model Part 3: Comminution equipment modelling

Fengnian Shi

The University of Queensland, Sustainable Minerals Institute, Julius Kruttschnitt Mineral Research Centre, 40 Isles Road, Indooroopilly, Brisbane, Qld 4068, Australia
Email address: f.shi@uq.edu.au; Telephone: +617 3365 5913; Fax: +617 3365 5999

ABSTRACT

It has been 10 years since the JK size-dependent breakage model was developed (Shi and Kojovic, 2007). This series of papers present 20 applications of the model for the mineral and coal industries. Part 3 of this series reviews its application to modelling comminution equipment. It is demonstrated that the JK size-dependent breakage model not only can be used for modelling particle breakage, but also can be employed as a basic structure for modelling comminution equipment. This is different to the traditional equipment modelling approaches, in which the population balance models are dominant. In this energy-size reduction modelling approach, the JK size-dependent breakage model provides a key mathematical template to rationally link the size reduction as the equipment model output with ore breakage property and specific energy as the two model inputs. Five case studies are reviewed, which includes modelling of a hammer mill for coke feed preparation, a vertical spindle mill for coal pulverised fuel grinding, a ball mill for batch grinding and continuous operation, HPGR simulations based on piston press testing data, and high voltage pulse disintegration of ores. A common feature of these models is that they all incorporate the measured material breakage characteristic parameters and machine operational conditions that are represented by the size-specific energy relation. The energy-size reduction modelling approach permits the simulations of the effects of changes in ore/coal and machine operating conditions on comminution product size distribution.

Keywords: Breakage characterisation; Size effect; Modelling; Energy efficiency.

1. Introduction

The population balance model has been widely used as a basic structure in modelling of grinding mills for the mineral and coal industries (Kelsall and Reid, 1965; Herbst and Mika, 1970; Austin, 1971-1972; Herbst and Fuerstenau, 1973, 1980; Whiten, 1974; Austin et al., 1984). The population balance model is based on a rate-size balance around a mill with two sets of breakage functions: a specific rate of breakage function and a breakage distribution function. Since the model parameters are simultaneously fitted to the mill feed and product data, the fitted (or back-calculated) parameters are interrelated, and it is difficult to decouple the machine-dependent and material-dependent effects. This limits the ability to do simulations of mill response to the variation in mill feed properties. Other researchers have criticised the fact that the traditional population balance model has no intrinsic capabilities to allow for simulating the process under conditions that are different from those that were used to fit its parameters (Carvalho and Tavares, 2013).

The swing hammer mill model published by Callcott (1960) is an early version of the population balance model presented in a vector form. The model incorporates three vectors: the selection vector, $\boldsymbol{S}$, the breakage vector, B, and classification vector, $\boldsymbol{C}$. Values of each element in the three vectors were manually adjusted for the model to represent the product size distribution. Thus for a product with 9 size fractions (i.e. 9 constraints for model fitting), the model offers 27 (3 vectors x 9 elements) adjustable parameters. Since the model parameters are less defined, it is difficult to establish a genuine relationship between these vectors and the machine operating conditions to predict hammer mill performance from the machine settings and the given feed.

The JKMRC (Julius Kruttschnitt Mineral Research Centre) ball mill model is based on a perfect mixing assumption (Whiten, 1974). This is a mill content based model, usually expressed as a

rate-size balance of mill contents under a steady-state. Morrell et al. (1993) demonstrated that the JKMRC model can lead exactly to the population balance model. One of the distinguishing features of the JKMRC models compared to the traditional population balance model is that the ore-specific appearance functions are physically measured, allowing the fitted model parameters to better reflect the operational conditions, thus decoupling the machine-dependent and material-dependent effects.

In the aforementioned models, the rate-size balance is merely based on the size distributions of mill feed and product, regardless of mill geometry and operational conditions. Although physical significance was assigned to some of the fitted model parameters by various researchers, the model itself is presented by a mathematical balance, and the grinding mill is treated as a "black box". It is argued that a model for comminution should be based on an energy-size reduction relationship, rather than merely on the rate-size balance. Any variations in mill (or equipment) geometry and operational conditions can be reflected in the energy input and the efficiency to deliver the energy for size reduction. Therefore a model taking into account both energy input and size reduction output would be more rational than those that only take account of the size reduction output without the energy input.

The energy-size reduction relationship has been used by many researchers and engineers to describe particle breakage, such as the three comminution laws by von Rittinger, Kick and Bond (Hukki, 1962), the various relationships presented by Rumpf (1973), Weichert (1988), King and Bourgeois (1993), Tavares and King (1998), Morrell (2004), Vogel and Peukert (2003), the JK breakage model (Napier-Munn et al., 1996), and the JK size-dependent breakage model (Shi and Kojovic, 2007). Traditionally, all these relationships were used to model a particle breakage event (either breakage probability or size reduction). Since in any comminution equipment, size reduction is resulted from the applied energy, it is believed that the energy-size reduction approach not only can be used for modelling particle breakage, but also can be applied for modelling comminution equipment. The author and his colleagues

have endeavoured to use this energy-size reduction approach to model comminution equipment in the past. In such a modelling exercise, the JK size-dependent breakage model provides a useful tool. In fact, it serves as the core equation in some of the equipment models developed at the JKMRC, since this model describes size reduction output as a function of two identified input variables – ore specific breakage property and machine related specific energy. Part 3 of this review presents five case studies to demonstrate how the energy-size reduction approach, together with the JK size-dependent breakage model, is implemented in modelling comminution equipment and processes.

2. Hammer mill modelling

Swing hammer mills have been used for a long time in the Australian coal industry to prepare coke oven feed. When feed particles drop into the path of the hammer tip circle (Fig. 1), some particles are severely shattered by the high-speed hammers. These products may be further broken again by the high velocity impact of particles on the breaker plates and breaker bar. The broken particles pass through the gap between the breaker bar and the hammer tip circle and land on an under-screen. Three typical orientations of screen apertures that can be selected include longitudinal, lateral and diagonal (relative to the particle flow direction). Aperture size of the under-screen can also be selected. Particles smaller than the screen aperture may be discharged through the under-screen and become the hammer mill product. Oversize materials will be carried over by the swing hammers into the breakage zone, and hence be subjected to further breakage. This size reduction process repeats until the particles are discharged through the under-screen. At steady-state there will be a charge of coal particles in the mill, drawing power in their movement and breakage.

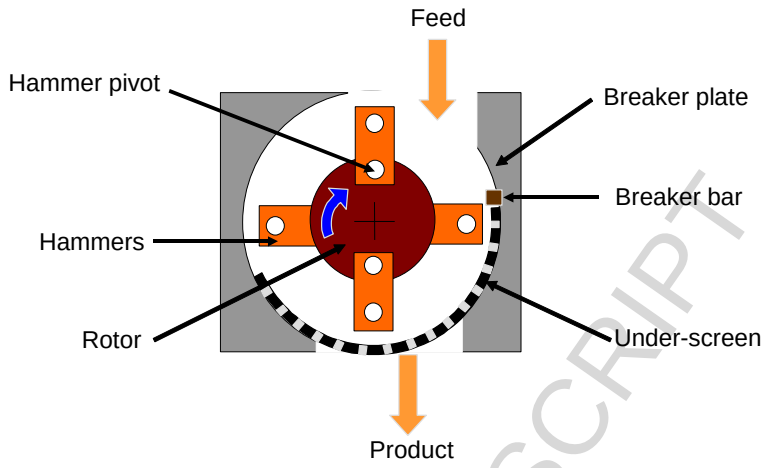

Fig. 1. Schematic diagram of the pilot-scale BJD swing hammer mill (Shi et al., 2003)

An energy-based swing hammer mill model was developed by Shi et al. (2003). This model consists of a crusher model with a dual classification function and a mechanistic power model to determine the dynamic internal recirculating load. This was perhaps the first trial by the author and colleagues using the energy-size reduction approach to model comminution equipment. The so-called energy-based model is distinguished in two aspects: i) a power model was developed to calculate the dynamic recirculating load; ii) the hammer mill product size distribution is calculated from a relationship between the applied specific comminution energy and the breakage distributions established from a single particle breakage test.

From the detailed experimental data using a pilot scale hammer mill, it was observed that the amount of fines in the product is positively correlated with mill power input, indicating that the use of under-screen causes recirculation, which offers more opportunity for particles to be broken finer by repetitive impacts, and the mill thus consumes more power. Callcott (1960) showed the motion of coal particles inside the BJD hammer mill using high-speed cine camera studies. Based on the assumption that the majority of mill power is consumed to rotate the fluidised coal inside the mill chamber, the hammer mill was modelled as a fan consuming power when moving a gas (Shi, 2002).

Using the law of conservation of energy and Bernoulli's equation, the net power that the mill consumes to rotate the fluidised coal and to force it through the breaker gap can be calculated as:

$$P_{net} = \left\{(P_1 - P_2) + (F + R) \cdot \left[\frac{\overline{V}_1\left(\frac{\overline{V}_1}{\overline{V}_2} - 1\right)}{2A}\right]\right\} \cdot \left(\frac{F+R}{SG}\right) \quad (1)$$

where P_{net} (kW) is net power draw, $(P_1 - P_2)$ (kPa) is static pressure before and after the fluidised coal passes through the gap between the hammer tip and the breaker bar, F (t h^{-1}) is the new feed rate, R (t h^{-1}) is the recirculation load, $\overline{V}_1$(m s^{-1}) is mean velocity of fluidised coal approaching to the breaker gap, $\overline{V}_2$ (m s^{-1}) is mean velocity of fluidised coal passing through the breaker gap, A (m^2) is the cross section area of the fluidised coal in the mill chamber, and SG (t m^{-3}) is coal solids density.

In a swing hammer mill, the static pressure is not possible to measure, so assume a parameter $m_1 = P_1 - P_2$. The velocities $\overline{V}_1$ and $\overline{V}_2$ are a function of the hammer mill rotor speed, the height between the feeder and hammer tip circle, the shape and location of the breaker plate, the gap of the breaker bar, the size distribution of the new feed and the recirculation, the moisture of the feed material, etc. The cross section area A is mainly a function of machine geometry. Let parameter $m_2 = \dfrac{\overline{V}_1\left(\dfrac{\overline{V}_1}{\overline{V}_2} - 1\right)}{2A}$; Eq. (1) then simplifies to:

$$P_{net} = \left[m_1 + m_2(F + R)\right] \cdot \left(\frac{F + R}{SG}\right) \quad (2)$$

Parameters m_1 (kPa) and m_2 (s^{-1} m^{-1}) can be calibrated by fitting Eq. (2) to the data of a given hammer mill without using screens, assuming R = 0.

By expanding Eq. (2), the net power that the hammer mill consumes appears to be a second-order polynomial function of the fluidised coal flow that consists of new feed and the

recirculating load. Eq. (2) can then be solved for the recirculating load, *R*, eliminating the negative sign in front of the square root:

$$R = \frac{-(m_1 + 2m_2F) + \sqrt{(m_1 + 2m_2F)^2 - 4m_2(m_2F^2 + m_1F - P_{net} \cdot SG)}}{2m_2} \quad (3)$$

As long as the two model parameters, m_1 and m_2, are calibrated for a particular hammer mill, then given the new feed rate, the net power draw and the solids density, the recirculating load can be calculated by Eq. (3).

A model with a dual-classification function was proposed based on the operating mechanisms of the swing hammer mill. Fig. 2 shows symbolically the parts of this hammer mill model and the internal flows between them. The model describes the process in such a way that a particle entering the milling chamber can be selected for breakage, or drop through the breaker gap onto the under-screen. The broken particles then have a similar chance of being broken further or dropping through the gap onto the under-screen. Particles reporting to the under-screen are subject to another classification: some particles are discharged from the under-screen as hammer mill product, and some are recirculated and subject to further breakage. Thus, the hammer mill is simplified to a single breakage zone and dual probabilities of entering or re-entering this breakage zone. The vectors ***f,*** ***x***, and ***p*** give the flow rates in each size fraction. The matrix ***B*** gives the relative distribution of each size fraction after being broken and the diagonal matrices $\boldsymbol{C_1}$ and $\boldsymbol{C_2}$ give the proportions of particles entering the breakage region. Details of the two classification functions are given in Shi et al. (2003).

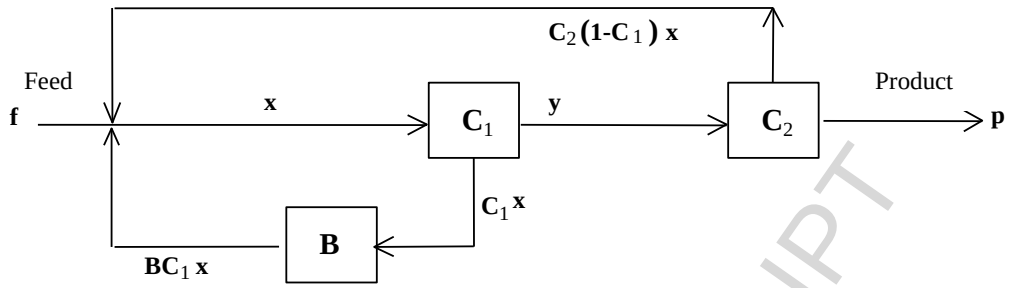

Fig. 2. Symbolic representation of the hammer mill model (Shi et al., 2003)

The breakage matrix ***B*** is material-specific, and should be measured, rather than being fitted as in the procedures of the population balance model or Callcott's hammer mill model (Callcott, 1960). Breakage characterisation on individual lithotype coals and the blended feed was conducted using the Drop Weight Tester (DWT), which is an impact tester with controlled kinetic energy. Three size fractions were tested for each type of coal: 8–16 mm, 22.4–31.5 mm and 45–50 mm. Energy imparted to the coal was varied from 0.01 kWh t^{-1} to 0.074 kWh t^{-1}. The product size distribution can be represented by a family of curves using marker points on the size distribution defined as the percentage passing at a fraction of the parent particle size (t_n) (Narayanan and Whiten, 1988). To make use of this description of coal particle breakage, marker points t_2, t_4, t_{25}, t_{50} and t_{75} are stored in matrix form against specific comminution energy, E_{cs}, for different initial coal particle size fractions. Table 1 shows typical breakage distribution matrices for the industrial hammer mill blend feed tested with the DWT.

Table 1. Breakage distribution matrix of the hammer mill feed determined by the single particle breakage DWT test (Shi et al., 2003)

Size (mm)	E_{cs} (kWh t^{-1})	t_{75}	t_{50}	t_{25}	t_4	t_2
8 -16	0.01	2.12	2.66	3.38	6.46	14.80
	0.025	2.40	3.09	4.33	11.65	27.26
	0.075	3.16	4.92	7.74	26.11	48.93
22.4 – 31.5	0.01	1.71	2.02	2.63	5.62	13.51
	0.025	3.26	4.00	5.57	16.76	35.05
	0.075	5.51	7.14	10.98	36.66	68.94
45 - 50	0.01	1.72	2.07	2.86	7.37	16.91
	0.025	3.07	3.87	5.77	19.19	40.54
	0.075	5.57	7.28	11.44	41.39	77.79

The breakage matrices presented in Table 1 appear different in two aspects compared with the traditional breakage appearance function used in the JKMRC crusher model. The traditional appearance function is formatted with t_{10} versus t_n values, where t_{10} is set at 10, 20 and 30 respectively. In the hammer mill model, specific energy E_{cs} is utilised (Column 2) in lieu of t_{10} used in the crusher model. This change allows a direct representation of the energy-size reduction relationship in the hammer mill model. E_{cs} is treated as a model parameter that is fitted to hammer mill survey data. For the BJD pilot scale hammer mill, the fitted E_{cs} was found to be 0.21 kWh t^{-1}. In separate research work, Djordjevic et al., (2003) conducted discrete element modelling (DEM) of hammer mills. The DEM calculates the total cumulative energy applied to each particle, including various forms of energy due to collisions between impellers and particles, particles and breaker bar, and particles to particles. Interestingly, the total specific energy Djordjevic et al. determined by DEM was 0.23 kWh t^{-1} for the BJD pilot scale hammer mill. This is very close to the fitted model parameter E_{cs} of 0.21 kWh t^{-1}.

The second difference is in the way to incorporate the particle size effect on breakage in the hammer mill model. The traditional crusher model only uses one map of the t_{10} vs t_n appearance matrix, derived from one single feed size. This implies that all particles in various

size fractions will be broken in the same way, and will appear in the product with the same size distribution. There is evidence of a particle size effect on breakage to oppose this assumption, showing that large particles will be broken with greater t_n values (Banini, 2000). The data presented in Table 1 acquired from single particle DWT impact tests also support this trend (except the 8-16 mm at 0.01 kWh t^{-1}). However, at the time when the hammer mill model was developed, the JK size-dependent breakage model had not been developed yet, and there was no validated breakage model available to represent the particle size effect on breakage. Therefore, three maps of E_{cs}-t_n appearance matrices for three feed particle size fractions were incorporated in the hammer mill model, as shown in Table 1. For a given feed size fraction and a specific energy level, a cubic spline function is used to interpolate or extrapolate the corresponding t_n values from the three maps of breakage appearance matrices.

There is a limitation using three maps of breakage appearance matrices to represent particle size effect. Since the breakage appearance matrix for each size is determined separately without a logical link of each other to represent its true effect, experimental errors may obscure the trend of the true size effect. After the JK size-dependent breakage model was developed, the DWT data used to generate the breakage distribution matrices presented in Table 1 were used to fit the JK size-dependent breakage model, with three model parameters determined: M = 24.5, p = 1.959, q = 0.717. The model fitting results are presented in Fig. 3. With the three characteristic parameters (M, p and q) and the t_n-t_{10} family of curves, the breakage distribution matrices presented in Table 1 can be replaced by the JK size-dependent breakage model. The advantage using the JK size-dependent breakage model to replace the three breakage distribution matrices is that the hammer mill model can describe the particle size effect on breakage better, leading to an improved overall prediction accuracy.

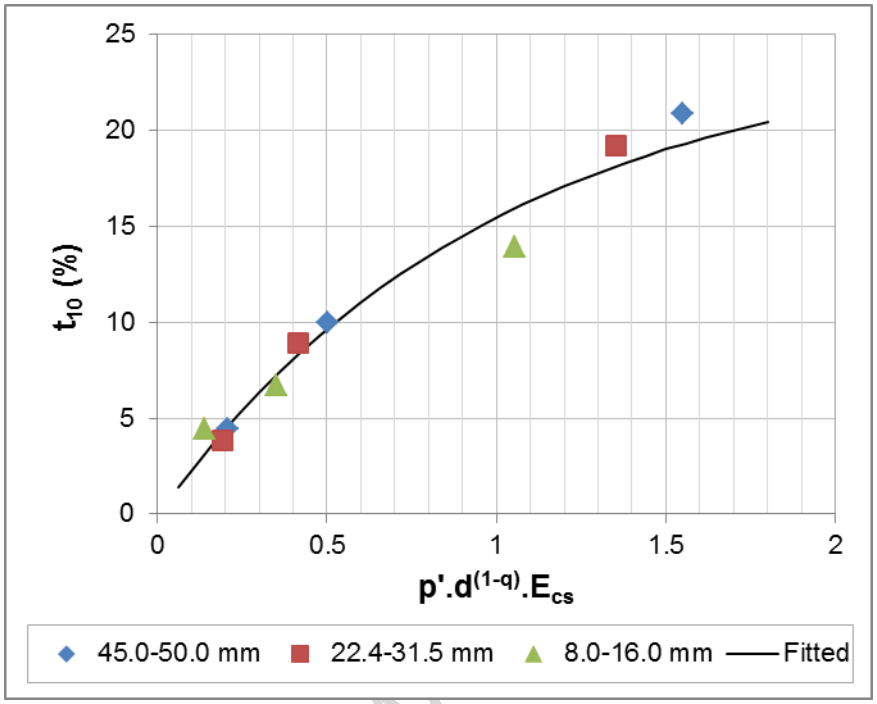

Fig. 3. The JK size-dependent breakage model fitted to the hammer mill breakage data

3. Vertical spindle mill model

The Vertical Spindle Mill (VSM) is one of the most widely used grinding devices for pulverised fuel (PF) generation in coal-fired power stations worldwide. According to published figures, coal pulverisation is an energy intensive process. Approximately 0.5 to 1% of gross power generation from coal fired power stations is consumed in coal grinding.

A VSM typically incorporates a grinding unit and an air classifier in a confined mill shell, operated under elevated pressure and elevated temperature. A schematic of a VSM ball-race design E-mill is shown in Fig. 4. The pulveriser is air-swept in which the coal is fed onto a rotating table through a central pipe. The coal is thrown outward by rotation into the grinding race. Seated in the race are ten 700 mm diameter steel balls (E-mill), or three rollers (MPS), which are held in the race by an upper stationary spider. The balls (or rollers) rotate with the table and pulverise the bed of coal that forms in the race, which is controlled partly by a

hydraulic loading system that adjusts the grinding pressure exerted by the spider through the balls (or roller) on the table. Primary air enters the pulveriser through jets arranged circumferentially outside the grinding table, and where the ground coal is pushed radially outward into the primary air flow, which entrains the coal.

Both E-mill and MPS pulverisers have two stages of classification in which oversize coal returns onto the grinding table. The first stage of classification is a simple elutriator which effects a crude classification of large coal fragments which have a terminal velocity exceeding the upward air velocity at this point in the device. The second stage of classification is a true gas cyclone which operates with inlet vanes and relies on the swirl to further classify the coal. The final PF exiting the gas cyclone will meet the required product size (70% < 75 µm).

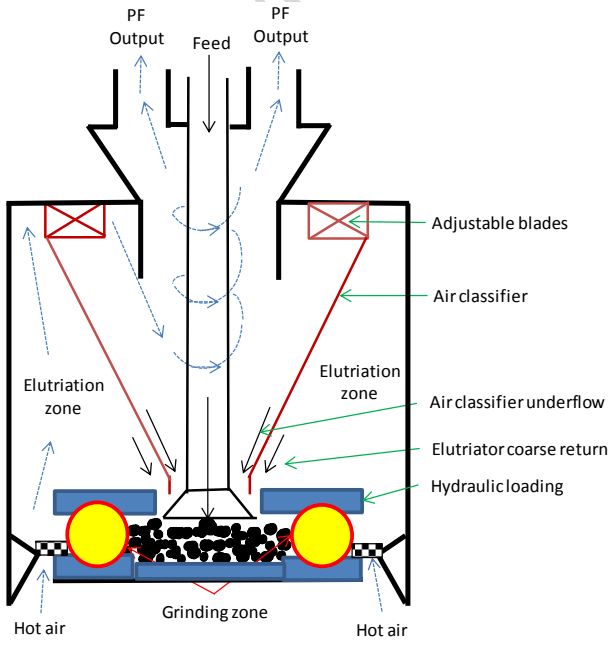

Fig. 4. Schematic of the grinding, elutriation and main classification zones in an E-mill (Shi et al, 2015a)

A VSM model was developed at the JKMRC (Shi et al., 2015a; Kojovic et al., 2015). The JKMRC VSM model takes a different approach to that in the literature using the population balance modelling method (Austin et al., 1982; Sato et al., 1996; Shoji et al., 1998). In these modelling processes, the mill was treated as a "black box", with its parameters being determined from the mill external sampling data (feed and ground product). The fitted

breakage rate parameters were then scaled up to run simulations for a full scale VSM operation in steady state. As this modelling approach did not directly incorporate mill geometry data and operational conditions in describing the mechanisms of particle breakage, transportation and classification, its success in optimisation of the pulveriser operation may be limited.

The JKMRC VSM model consists of three basic functions: comminution, elutriator classification and air classification. These functions are in effect linked in a grinding-classification circuit and the model structure (which effectively is the circuit flow sheet) is shown in Fig. 5. A key requirement in defining the three functions is the internal stream data; without such data, the VSM model becomes a "black box" model, too. The VSM mill internal sampling technique developed by Sligar (1975) was improved by the JKMRC (Ozer et al., 2009) in an Australian power station E-mill surveys. The sampling technique was further modified by the CUMT (China University of Mining and Technology) and utilised in a Chinese power station for surveys of a ZGM mill (A Chinese localised roller-race VSM) (He et al., 2011).

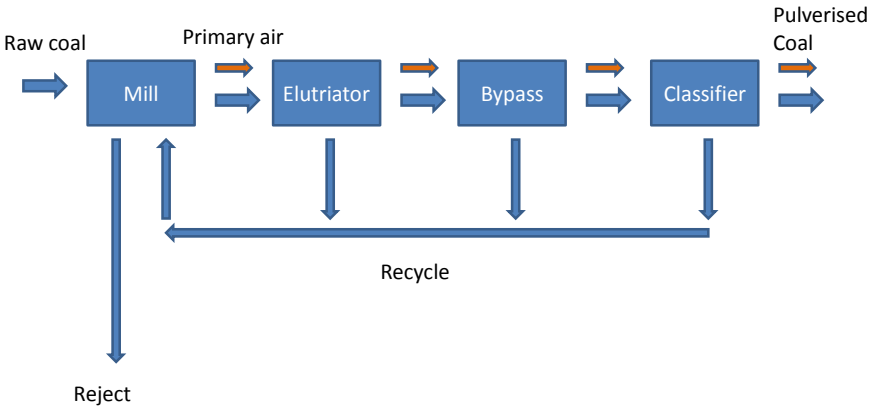

Fig. 5. The JKMRC VSM model structure for E-mill and MPS mill

The comminution function (Mill in Fig. 5) will be reviewed in this paper to demonstrate the modelling approach using the energy-size reduction relationship and the JK size-dependent breakage model for the VSM model. Classification in the elutriator was modelled using a Rosin-Rammler efficiency curve, and the air classifier was modelled using Sproull's gas

cyclone model (Sproull, 1970). Details of the two classification functions can be found in Shi et al., (2015a) and Kojovic et al. (2015).

In order to use the energy-size reduction approach to model the VSM, three sub-models for the comminution function were developed: mill power draw model, size specific energy model, and particle breakage model.

The mill power draw, P_m (J s^{-1}), is modelled from physical principles: P_m = torque x angular velocity, where torque is calculated as

$$\tau = F \cdot \mu \cdot R \cdot n_b \tag{4}$$

and angular velocity is calculated as

$$\omega = \frac{2\pi \cdot N}{60} \tag{5}$$

where τ (N.m) is the mill torque, F (N) is the force acting on each ball/roller, μ is the friction coefficient, R (m) is the radius of rotation, n_b is the number of balls (or rollers), ω (radian s^{-1}) is the angular velocity, and N (revolution min^{-1}) is the grinding table (race) rotational speed.

Based on the survey data collected from the E-mill operated at the Australian power station, a model for the frictional coefficient was developed. This model takes the following form:

$$\mu_{net} = C_1 \left\{ 1 - exp\left[-\left(\frac{GTF}{C_2} * Fine^{C_3} \right) \right] \right\} \tag{6}$$

where μ_{net} is the predicted friction coefficient of 10 balls on the coal bed, GTF (t h^{-1}) is

grinding table total feed rate, *Fine* is % passing 75 μm in the *GTF*. Both *GTF* and *Fine* are estimated from the mass balanced mill internal sampling data. C_1, C_2 and C_3 are parameters fitted to six sets of power station survey data: C_1 = 0.1337; C_2 = 848.6 and C_3 = 0.4509. GTF/C_2 is the race filling fraction. The total friction coefficient (μ_{total}) reflects the non-load friction ($\mu_{non\text{-}load}$) plus balls on coal bed friction (μ_{net}). When *GTF* = 0, Eq. (6) indicates μ_{net} = 0, so that $\mu_{total} = \mu_{non\text{-}load}$.

The survey data collected from the E-mill in Australia and ZGM mill in China all indicated that breakage varied with particle size. This is attributed both to grinding conditions (reflected by the size-specific energy) and the inherent material properties. The VSM model was therefore constructed with incorporation of two factors for particle size reduction.

Considering the specific energy E_{cs} applied to material on the grinding table, one would expect that small particles will be compressed in the bed by the balls and their movement. The contact area and size of particles should control the intensity of breakage of fine particles trapped in the bed. The stress on coarse particles would be lower but there would be a finite E_{cs} limit that any particle might be subjected to. To represent this mechanism the following breakage model form was proposed: $E_{cs} \propto$ Area/Volume, leading to $E_{cs} \propto 1/d$. A simple expression was proposed:

$$E_{cs} = E_{cs0} + \frac{b}{d^c} \tag{7}$$

where *d* (mm) is the average coal particle size defined as the geometric mean size of the adjacent two screen apertures, and E_{cs0} (kWh t^{-1}) is the effective E_{cs} applied to the coal on the grinding table and could be calculated using the expression:

$$E_{cs0} = \frac{P_{net}}{K \cdot GTF} \tag{8}$$

where P_{net} (kW) = net power drawn by mill = gross power – no-load power, K is an inefficiency calibration constant fitted to survey data, and b, c are model constants, fitted to the survey data (b = 0.133, c = 1.016).

The K constant in Eq. (8) represents an inefficiency factor, which was found to be linearly related to air mass flow rate, suggesting that the specific energy decreases with increasing air rate due to the higher recycle loads. The constant c was found to be very close to 1, which supports the assumption that the E_{cs} is inversely related to size. The form of the E_{cs} model is illustrated in Fig. 6, showing the significant increase in E_{cs} as particle size is reduced. The E_{cso} value for this particular survey condition was 0.275 kWh t^{-1} (P_{net} = 174 kW calculated by Eqs. (4-6), GTF = 245 t h^{-1}, K = 2.58).

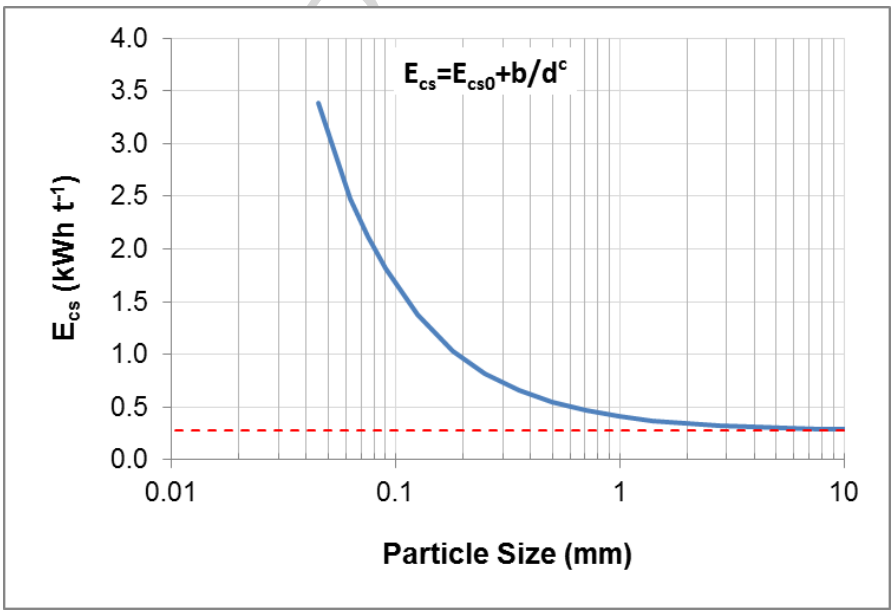

Fig. 6. Specific energy (E_{cs}) vs particle size relation used in VSM comminution model (Shi et al., 2015a)

In terms of incorporating the inherent material property of size-dependent breakage nature in the VSM model, the authors were in a better position than at the time when the hammer mill model was developed (Section 2). The JK size–dependent breakage model had been developed, and was available to be incorporated in the VSM model. The JK size-dependent

breakage model (Eq. (9)) serves as the core equation linking the grinding conditions (size-specific energy) and the inherent particle breakage properties (*M, p* and *q*):

$$t_{10(i)} = M\{1 - exp[-3.6p \cdot d^{(1-q)} \cdot k(E_{cs(i)} - E_0)]\} \quad (9)$$

where $t_{10(i)}$ (%) is a breakage index defined as product cumulative passing 1/10th of initial feed size for size fraction *i*, *d* (mm) the initial particle size, *k* the successive number of impacts with the single impact energy, $E_{cs(i)}$ (kWh t^{-1}) mass specific energy for size *i*, and E_0 (kWh t^{-1}) energy threshold. The three model parameters, *M, p and q,* in Eq. (9) are determined from one set of breakage test data using a fine particle breakage characteriser (JKFBC, Shi and Zuo, 2014). The size-specific energy, $E_{cs(i)}$ that is calculated by Eqs. (4-8), is then used to calculate $t_{10(i)}$ values for each size fraction based on Eq. (9) and the coal breakage parameters *M, p* and *q*.

The energy based size reduction model for comminution, together with the elutriator, by-pass and air classifier models, are implemented in an Excel-based MDK (Model Development Kit) version of the VSM model. Implementation of simulation models in the MDK is an approach used for model testing at the JKMRC. Fig. 7 shows the VSM model in the Excel simulator for the E-mill and the quality of model fitting to the mill internal and external stream data.

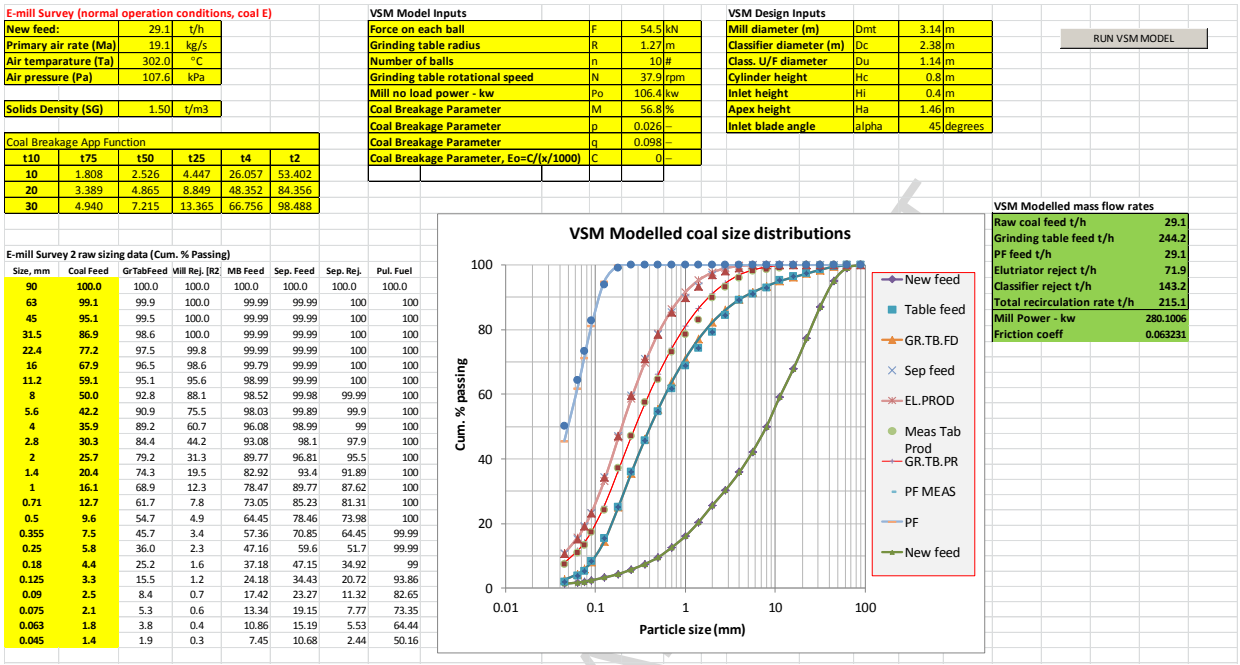

Fig. 7. Excel mill simulator interface for VSM E-mill, with four fitted model parameters to produce the size distributions

4. Specific energy based ball mill model

The ball mill is widely used in the mineral, cement and coal industries for primary, secondary, tertiary and regrinding duties. As discussed in the Introduction, the population balance model is typically employed for ball mill modelling. The existing JKMRC perfect mixing ball mill model, developed by Whiten (1974) and implemented in the comminution software JKSimMet, is used extensively. The perfect mixing ball mill model is another form of the population balance model (Morrell et al., 1993). A number of limitations associated with this ball mill model have been identified, such as the use of a set of default breakage appearance functions for all ores, and the lumped model parameter R/D* for breakage rate and mass discharge rate.

In developing a specific energy based ball mill model, Shi and Xie (2015) first modelled the energy-size reduction relationship in batch grinding, in which there is no mass transport or discharge mechanism occurring, so as to decouple particle breakage from mass transport

and discharge classification. This energy-size reduction relationship is then applied in full scale continuous ball mill operation, by adding discharge function into the batch grinding model (Shi and Xie, 2016).

Following the present author's modelling concept, a specific energy-size reduction function (Eq. (9)) was utilised for the batch grinding ball mill model. This model first calculates the particle breakage index, t_{10}, according to size-specific energy, and then the product size distribution using the t_{10}-t_n relationships and the mass-size balance approach. Symbolically, the mass-size balance, or mass conservation, can be expressed by Eq. (10).

$$p_i = \sum_{j=1}^{i-1} \mathrm{f_i} \cdot \mathrm{m_{ij}} \tag{10}$$

where f_i and p_i are the mass fractions of size i in the mill feed and product, and m_{ij} is a lower-triangular breakage matrix, indicating the mass fraction of appearance of size i material produced by fracture of size j material. For each size i, the summation sign sums up the total material from sizes larger than i to size i-1. Fig. 8 exhibits an example of the lower-triangular breakage matrix m_{ij} determined by the method described below.

Size (mm)	2.800	2.360	2.000	1.700	1.180	0.850	0.600	0.425	0.300	0.212	0.150	0.125	0.106	0.090	0.075	0.063	0.053	0.045	0.038
3.350																			
2.800	0.3409																		
2.360	0.2085	0.3446																	
2.000	0.1289	0.2096	0.3480																
1.700	0.0801	0.1288	0.2105	0.3514															
1.180	0.0847	0.0797	0.1288	0.2115	0.3564														
0.850	0.0296	0.0837	0.0793	0.1287	0.2128	0.3637													
0.600	0.0213	0.0290	0.0827	0.0789	0.1286	0.2147	0.3706												
0.425	0.0186	0.0208	0.0284	0.0818	0.0783	0.1284	0.2164	0.3778											
0.300	0.0160	0.0182	0.0204	0.0278	0.0804	0.0774	0.1281	0.2181	0.3849										
0.212	0.0135	0.0158	0.0179	0.0199	0.0269	0.0783	0.0765	0.1278	0.2197	0.3921									
0.150	0.0115	0.0132	0.0155	0.0176	0.0193	0.0256	0.0764	0.0756	0.1273	0.2212	0.3992								
0.125	0.0054	0.0112	0.0129	0.0152	0.0172	0.0184	0.0245	0.0744	0.0746	0.1268	0.2226	0.4049							
0.106	0.0045	0.0053	0.0110	0.0127	0.0149	0.0165	0.0176	0.0233	0.0724	0.0736	0.1263	0.2237	0.4084						
0.090	0.0042	0.0045	0.0052	0.0108	0.0124	0.0143	0.0159	0.0168	0.0222	0.0705	0.0726	0.1258	0.2243	0.4118					
0.075	0.0043	0.0041	0.0044	0.0051	0.0105	0.0119	0.0138	0.0154	0.0160	0.0211	0.0685	0.0717	0.1254	0.2249	0.4153				
0.063	0.0038	0.0042	0.0040	0.0043	0.0049	0.0101	0.0114	0.0134	0.0148	0.0152	0.0201	0.0670	0.0712	0.1251	0.2254	0.4189			
0.053	0.0034	0.0037	0.0041	0.0040	0.0042	0.0047	0.0097	0.0110	0.0129	0.0142	0.0145	0.0193	0.0661	0.0707	0.1248	0.2260	0.4224		
0.045	0.0029	0.0033	0.0036	0.0041	0.0038	0.0040	0.0045	0.0093	0.0106	0.0124	0.0137	0.0139	0.0188	0.0652	0.0701	0.1244	0.2265	0.4258	
0.038	0.0164	0.0028	0.0033	0.0035	0.0039	0.0037	0.0038	0.0044	0.0089	0.0101	0.0120	0.0133	0.0136	0.0184	0.0642	0.0695	0.1240	0.2270	0.4291
0.000	0.0015	0.0175	0.0199	0.0227	0.0254	0.0281	0.0305	0.0329	0.0357	0.0427	0.0506	0.0605	0.0722	0.0841	0.1002	0.1612	0.2271	0.3472	0.5709

Fig. 8. Example of the lower-triangular breakage matrix (m_{ij})

It is emphasised that in this modelling approach, the breakage rate used in the population balance model is excluded from the mass-size balance equation (Eq. (10)); instead, a breakage matrix, m_{ij}, is adopted in the mass-size balance calculation. The breakage matrix m_{ij} has three distinguishing features:

- Ore-specific: The ore breakage characteristic parameters are independently measured with the JKFBC from the ball mill feed sample (referring to Section 7 in Part 1 of the review paper (Shi, 2016)), rather than using a default appearance function.
- Size-dependent: Particle size effect on breakage is measured through the JKFBC tests and described by the JK size-dependent breakage model parameters *M, p* and *q* (Eqn. 9). Specific energy available for size reduction is also size-dependent.
- Specific energy-based: The breakage matrix m_{ij} is calculated based on the estimated specific energy, reflecting a breakage result from the combined effects of ore inherent breakage properties and the effective specific energy input to cause this size reduction.

To determine the breakage matrix in Eq. (10), two major input factors are considered in the model: the ore factor and the machine factor. This is similar to the VSM model reviewed in Section 3. The size reduction model incorporates two separate functions: the breakage function that describes the relationship between particle size reduction and input specific energy; and the selection function that describes the probability of particles in a given size fraction being selected for breakage.

The size-specific energy is used to determine particle size reduction in a ball mill. The size-specific energy is calculated from mill power draw divided by mass flow rate to give a mean specific energy. The mean specific energy is then used to calculate size-specific energy. The mill power is estimated by the Morrell power model (Morrell, 1992), which has the advantage of incorporating mill geometry and operational conditions in the ball mill model. From the power draw, grinding time and the particle mass in a batch grinding test, the mean

specific energy in batch grinding can be estimated. In a continuous mill, the mill power dividing the fresh mill feed rate gives mean specific energy.

It is hypothesised that the mean specific energy E_{cs} is not applied to all particles evenly in a ball mill. There is a selection function governing the size-specific energy level, some particle sizes receiving more specific energy, and some other sizes receiving less. The available specific energy for each particle size, $E_{cs(i)}$, is determined by a selection function S_i (Eq. (11)):

$$E_{cs(i)} = S_i \cdot E_{cs} \tag{11}$$

The selection function values (dimensionless) are treated as model parameters. Three S-values at three size spline knots were fitted. The cubic spline method was incorporated in the model to calculate the full size selection function from the three fitted knot values. The fitted selection functions for the three Bond ball milling cycles of Sample A are given in Fig. 9. Sample A is a gold-copper ore collected from an Australian gold-copper concentrator. The shape of the selection function indicates that the 0.6 to 0.8 mm particles in the Bond ball mill have a higher tendency to be selected for breakage. The probability of selection for breakage decreases for the particle sizes away from the peak size, particularly for the fine end. The shape of a selection function curve in a ball mill is dominated by ball charge size distribution and feed particle size distribution. For a given ball charge, a certain particle size is more easily broken than the other sizes. Since the Bond ball charge was identical in the seven cycles of grinding, the peak of the fitted selection function is similar. Note from Eq. (11), the selection function is used to define size-specific energy efficiency, which indicates that with the standard Bond ball mill charge, the mill has the optimal energy efficiency to break particles around 0.6 to 0.8 mm.

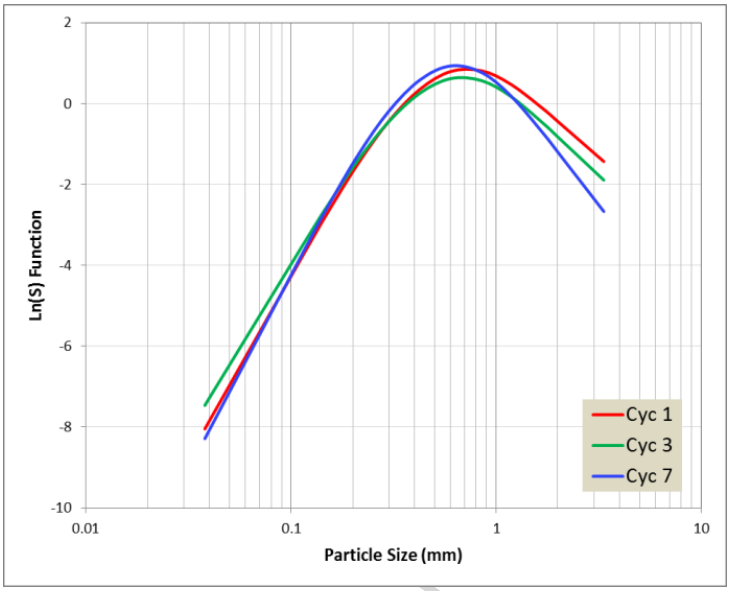

Fig.9. The fitted selection functions for three cycles of Bond ball mill test (Shi and Xie, 2015)

Once the specific energy-based size reduction model was proved to be able to work with batch grinding ball mill data, it was extended from batch grinding to full scale ball milling in continuous operation mode. A set of classification data collected by Man (2001) from the internal sampling of an operational ball mill reveals that the shape of the classification function in a ball mill is similar to the Whiten expression for corrected efficiency to overflow (Napier Munn et al., 1996). Therefore the Whiten efficiency equation was adopted and modified to describe the ball mill discharge function in the continuous ball mill model (Shi and Xie, 2016).

Data from two full scale ball mill operation surveys, one in a gold concentrator in Australia and one in PGM concentrator in South Africa, were used to validate the continuous ball mill model. The samples of the ball mill feed were tested with the JKFBC to determine the ore-specific breakage characteristic parameters *M, p* and *q*. These ore specific parameters were kept constant during model fitting. The specific energy based ball mill model fits the data well (Fig. 10), despite the very different feed size distributions and the product size distributions between the two ball mills in operation.

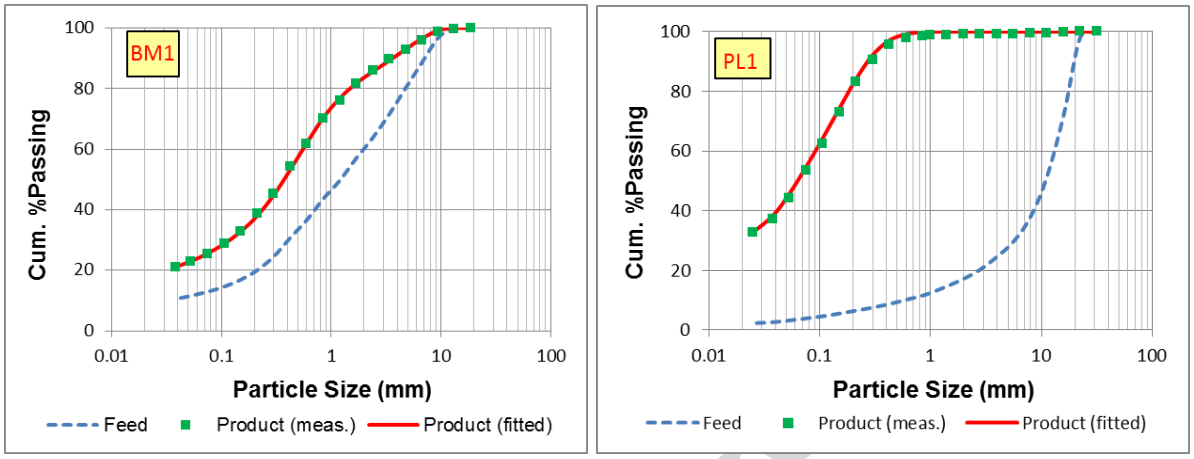

Fig. 10. Ball mill product size distributions fitted by the specific energy based ball mill model in comparison with the survey data (BM1 for a gold concentrator and PL1 for PGM concentrator) (Shi and Xie, 2016)

The model incorporates two separate functions: the selection function and discharge function, which allows investigation of these separate effects on ball mill performance. In the two PGM concentrator surveys (PL1 and PL2), the mill operational conditions were similar. The calibrated selection functions using PL1 were applied to PL2 (without fitting). The only three parameters fitted in PL2 were associated with the discharge function. The fitted discharge function parameters were found to be significantly different between PL1 and PL2 (Fig. 11). The D_{max} values (maximum discharge rate) are represented as the intercepts of the curves on the y-axis. The fitted D_{max} values were 312 h^{-1} and 231 h^{-1} for PL1 and PL2 respectively. The PL2 survey had finer feed and larger overall throughput than in PL1, but the discharge rate for fine particle size less than 0.06 mm was smaller than in PL1. Analysis of the fitted discharge rates suggests that this may be attributable to the higher grinding density in PL2 (77.2% solids in PL2 vs 74.3% solids in PL1). Associated with the high grinding density, slurry rheology may become an issue affecting the maximum discharge rate (D_{max}) for fines in PL2 (Shi and Napier-Munn, 2002). This interpretation of the model parameters tallies with the plant observation, though the authors were not involved in the plant surveys. Such capability of the specific energy based ball mill model is difficult to achieve using the lumped breakage rate and discharge rate parameters (R/D^*) in the traditional perfect mixing model or the population balance model.

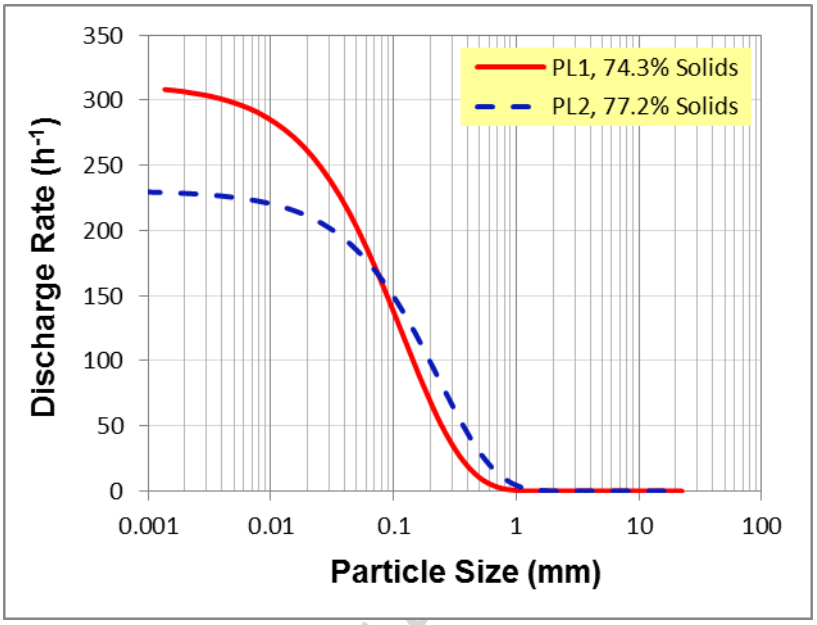

Fig. 11. The model fitted discharge functions, with the same selection functions being used in two surveys conducted at the PGM concentrator (Shi and Xie, 2016)

5. HPGR simulation model

In recent years, HPGR (High Pressure Grinding Rolls) has found wide application in the mineral industry, attributed mainly to its energy efficiency. Since sizing the HPGR often needs pilot scale HPGR tests, which requires large amount of ore samples and the associated testing costs, there is an incentive to use small scale testing to predict the energy requirement and the resultant product size distribution of the HPGR for a given ore.

Davaanyam (2015) and Davaanyam et al. (2015) of The University of British Columbia present a simulation method to predict the energy requirement of the HPGR and the size reduction result under compression. They used piston press testing on five narrow size classes of particles at three energy levels. The data collected are used to fit an energy–breakage model (Eq. (12)). The energy–breakage model was modified from the work of Shi and Kojovic (2007) by adding an exponent n to particle size x. As commented in Part 1 of

this review (Shi, 2016), this equation is coincidently the same equation as the JK size-dependent breakage model (Eq. (5a) in Part 1 when E_0 = 0 and q = *1-n*, which leads to *1-q equal to n*) developed 10 years ago.

$$t_{10} = M\left[1 - \exp\left(- f_{mat.} \cdot x^{n} \cdot E_{sp}\right)\right] \tag{12}$$

Other t_n values, which represent the percentage passing 1/nth of the initial particle size, can be determined from piston press product size distributions. Plotting t_n against t_{10} suggests that there is a set of master curves that describes the t_n–t_{10} relationships regardless of ore type as shown in Fig. 12. Therefore the whole particle size distribution after breakage can be reconstituted with knowledge of t_{10} alone. This confirms the findings of Narayanan and Whiten (1988).

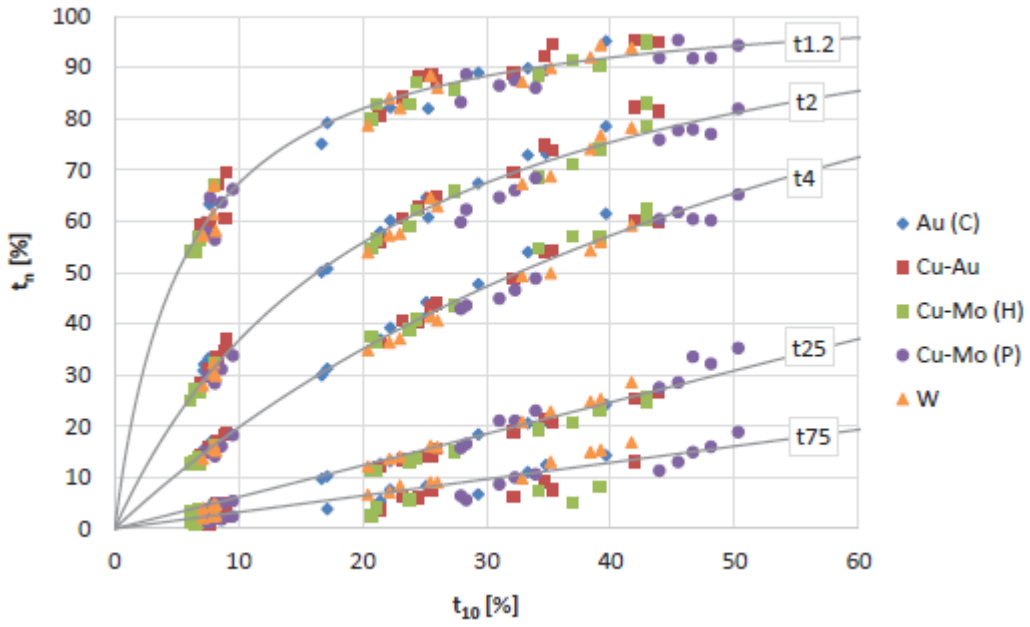

Fig. 12. A set of master curves describing t_n–t_{10} relationships (Davaanyam et al., 2015)

Once the energy–breakage relationship is defined by the piston press testing data on a given ore, and the set of master curves describing the t_{10} versus t_n relationship is known, the energy–size reduction performance of the HPGR can be simulated. In the simulation process, it is assumed that there are two breakage zones. Particles above a critical size, x_c, are pre-crushed, and below the critical size they are ground in a compression bed. This assumption is similar to Morrell et al. (1997a, b), with the exception that the coarser particles in the feed of this model are assumed to break by compressed bed mechanisms rather than by single particle impact breakage. Therefore Eq. (12) is used to calculate the size reduction index t_{10} by pre-crushing with a split of specific energy described below.

The product from the pre-crushing stage is combined with the finer fraction (below x_c) in the feed and the combined product is subjected to size reduction in the grinding stage. This arrangement in the simulation allows the coarse particles to break via both pre-crushing and grinding stages, while the fine particles break only via the grinding stage. It was found that the fines content in HPGR feed will affect the inter-particle breakage by bed compression. Eq. (12) was therefore modified to take account the effect of fines content in feed (Eq. (13)), which is used for the simulation of the breakage in the grinding stage.

$$t_{10} = \left(M - c \cdot P_{fines}\right) \cdot \left[1 - \exp\left(- f_{mat.} \cdot x^n \cdot E_{sp}\right)\right] \tag{13}$$

where c is a fitted constant to multiply by the percentage of fines (below x_c) in the feed, P_{fines}.

In the simulation, it was assumed that the total energy is distributed between the pre-crushing and the grinding stages. The energy to the pre-crushing stage is a function of the fraction of coarser particles in the feed, and the specific energy in the pre-crushing stage and the grinding stage is calculated using Eqs. (14) and (15). Note that there is a printing error in the original publications (Davaanyam, 2015; Davaanyam et al., 2015) that the sum

of the two stages of specific energy is not equal to the total specific energy. This error has been corrected in Eq. (14).

$$E_{sp}^{crush} = \beta_{split} \cdot f_{coarse} \cdot E_{sp} \tag{14}$$

$$E_{sp}^{grind} = E_{sp} \cdot \left(1 - \beta_{split} \cdot f_{coarse}\right) \tag{15}$$

where f_{coarse} is the coarse (above x_c) particle fraction in the feed, and β_{split} is a model parameter.

The simulation models have three parameters that were fitted to the data of 36 HPGR tests on five different ores: x_c = 16 mm, β_{split} = 0.157 and c = 1.08 (Davaanyam et al. (2015)).

The total specific energy, E_{sp}, in Eqs. (13-15) is unknown. A two-step approach was taken to estimate the specific energy used for HPGR: i) Estimate the required piston pressure by an empirical regression equation (Eq. (16)) to deliver the same specific energy into the sample as the HPGR; ii) Conduct piston press tests at the estimated pressures and integrate the resulting force-displacement curves to provide a prediction of net specific energy of HPGR.

$$P_{Piston} = 5.53 + 53.3F_{sp} + 24.3w - 86.2\rho_b + 13.1F_{50}^{H} - 44.4\frac{F_{50}^{H}}{F_{50}^{P}} + 2.98P_{1mm}^{P} \tag{16}$$

where P_{Piston} (MPa) is the estimate of required piston pressure, F_{sp} (N mm^{-2}) is specific pressing force, w (%) is moisture content, ρ_b (g ml^{-1}) is bulk density, F_{50} (mm) are 50% passing feed particle sizes for HPGR and piston press tests, and P_{1mm}^{P} (%) is percentage passing 1 mm in feed to piston press test.

The predicted specific energy for HPGR using this two-step approach is within ± 25% of the measured values. The simulated product sizes in terms of P_{80} and P_{50} for the 36 HPGR tests, in comparison with the measured values, are presented in Fig. 13.

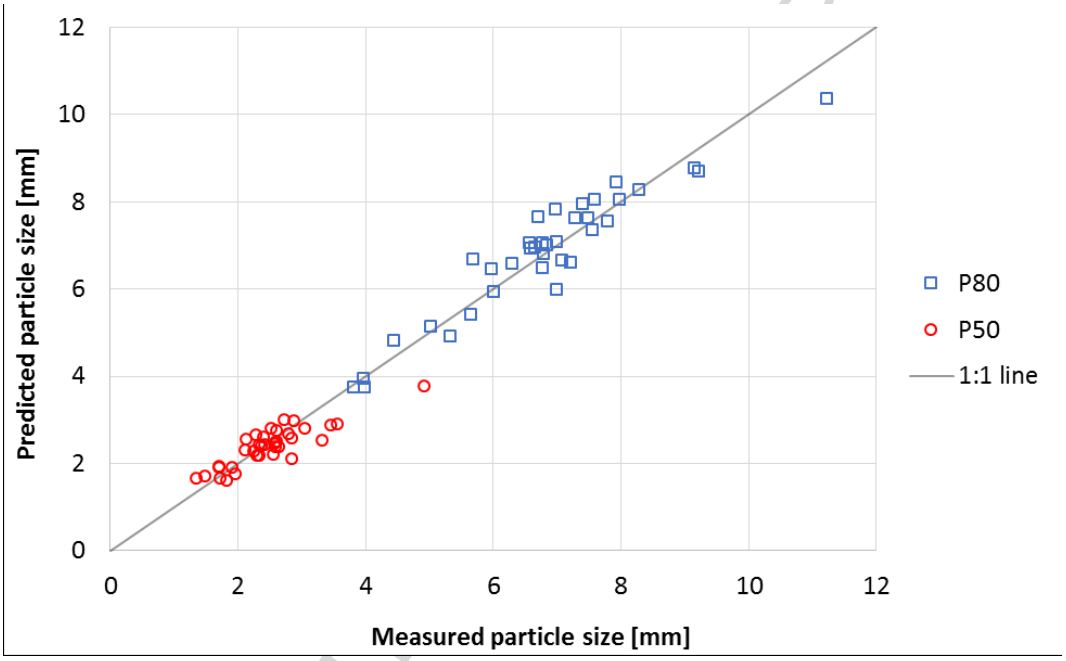

Fig. 13. Predicted product size of 36 HPGR tests (Davaanyam et al., 2015)

6. Modelling size reduction by high voltage pulse breakage

In order to improve the efficiency of existing comminution processes, various novel methods have been studied in the literature. One of these novel methods is high voltage pulse (HVP) breakage, a comminution method that uses high voltage pulses to initiate electrical breakdown inside ore particles, generating a strong tensile force to disintegrate the particles. Three potential applications of the HVP technology for the mineral industry were identified in the JKMRC investigations: Ore pre-weakening (Wang et al., 2011), preferential liberation and recovery of valuable minerals (Wang et al., 2012; Parker et al., 2015), and ore pre-concentration (Zuo et al., 2015a; Shi et al., 2015b). All these HVP applications involve particle size reduction. To predict their performance, one basic step is to model the

relationships between size reduction and HVP energy input. The JK size-dependent breakage model was again utilised (Zuo et al., 2015b). In the HVP application, it becomes simpler than the aforementioned modelling of mechanical comminution equipment, as the HVP specific energy is directly measured by the generator energy divided by ore sample mass in both batch tests and pilot scale tests. This exercise was the first time that the viability of the JK size-dependent breakage model applied in electrical disintegration in lieu of the traditional mechanical breakage has been investigated.

There are two distinct breakage modes when a particle is subjected to a single pulse discharge. If an electrical breakdown channel passes through the particle body and splits the particle into several fragments, this is called body breakage. If the electrical breakdown channel develops along the particle surface and generates a few chips (less than 90% of the parent particle mass), while the main body of the particle is unbroken and remains at the parent size fraction, this is called surface breakage. Two HVP breakage indices were used to describe HVP breakage behaviour: body breakage probability (the D_1-model) and body breakage product fineness (the D_2-model). The body breakage probability is defined as a percentage of the mass of body breakage product divided by the mass of initial feed. The breakage index, t_{10}, is used as the second index to describe product fineness and size distribution.

The two HVP breakage models take the same equation form (Eq. (17)).

$$D_n = M\left\{1-\exp\left[-3.6\,p_n \cdot d^{(1-q_n)} \cdot k\left(E_{cs}-E_0\right)\right]\right\} \tag{17}$$

where D_n is the HVP breakage indices defined above. When n = 1, D_1 (%) is body breakage probability; when n = 2, D_2 is t_{10}. E_{cs} (kWh t^{-1}) is HVP specific energy, calculated by pulse generator energy divided by ore mass treated. The pulse generator energy is determined by Eq. (18):

$$E_p = 0.5C \cdot U^2 \tag{18}$$

where E_p (J) is the pulse generator energy, *C* (F) is the capacitance and *U* (V) is the voltage of the pulse from a generator. Note that the pulse generator energy is determined by the HVP operational conditions – at a constant operational condition setting, the energy for each pulse is a constant. However, the spark energy that is the energy delivered to the ore sample is different from the pulse generator energy, which depends on the ore properties. In evaluation of HVP energy efficiency, the pulse energy from a generator (Eq. (18)) is often used, since this energy is usually greater than the spark energy. The energy efficiency to deliver the pulse energy from a generator to spark energy is referred in van der Wielen et al. (2013) and Zuo et al. (2015a).

The data collected from the tests on three ore samples using a pilot scale HVP installed in Switzerland (Zuo et al., 2015) were used to validate the HVP breakage model. Ore A was collected from a gold-copper mine operation located in New South Wales, Australia. The gold-copper mineralization occurs in quartz veins, sheeted quartz sulphide veins and as disseminations. Ore B was collected from a major copper, silver and gold mine in South Australia. The deposit is an iron oxide copper gold (IOCG) style mineralization. Ore C is a hematite ore with Fe grade of around 63.0%. It was observed that some particles were highly porous. Fig. 14 shows the fitting results of the two HVP breakage indices for the three ore samples. There are a nominal 27 data points for Ore A (3 sizes × 3 voltages ×3 energies), 6 data points for Ore B (3 sizes ×2 energies) and 9 data points for Ore C (3 sizes ×3 energies). All of these data points represented the HVP breakage testing results of particles subjected to a single pulse discharge.

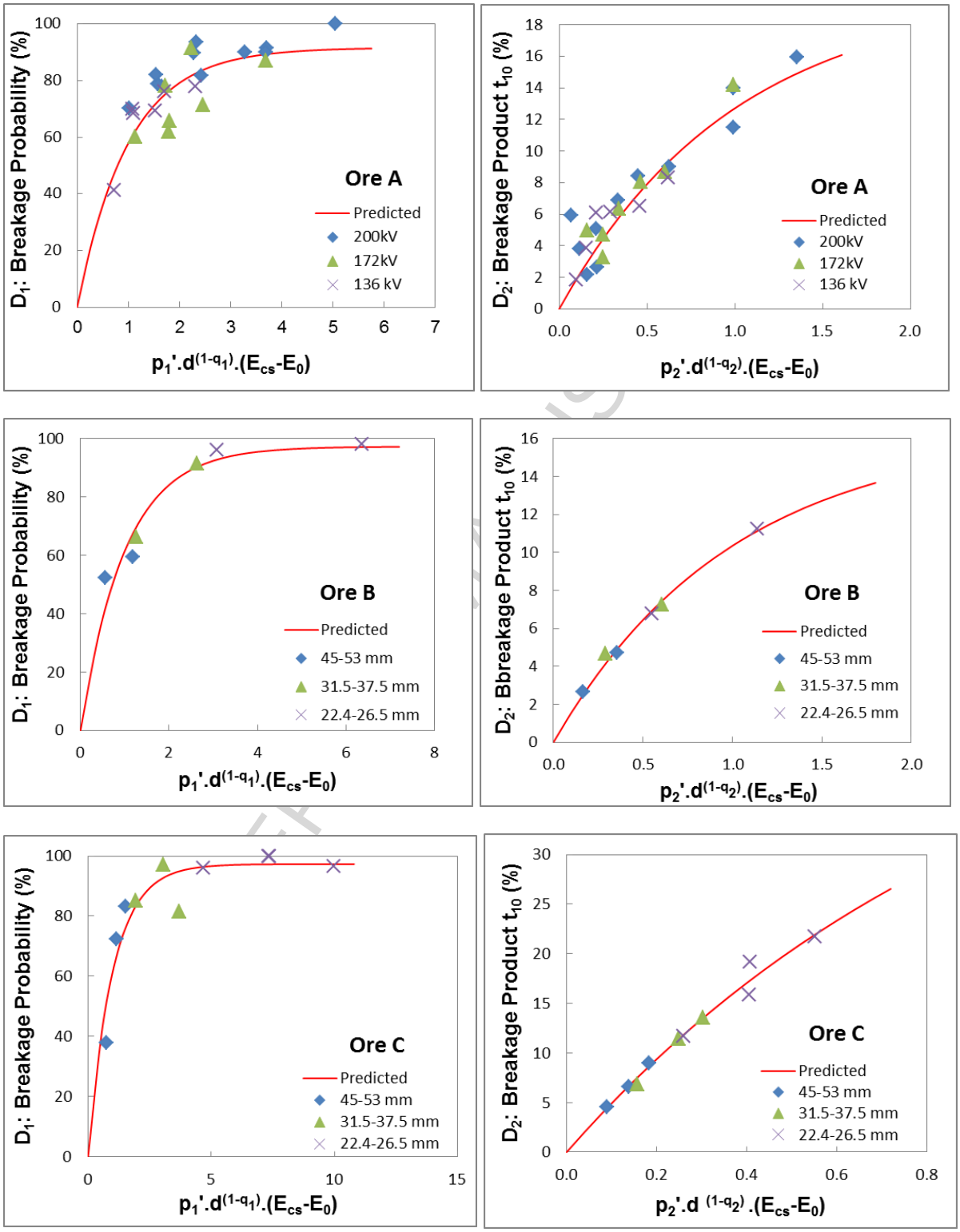

Fig. 14. The two HVP breakage models (left and right) fitted to the pilot scale testing data of three ore samples (Zuo et al., 2015b)

It is well known that ore breakage properties affect the mechanical breakage result. In the HVP breakage process, not only the mechanical breakage properties, but also the electrical

properties of the ore, will affect the breakage results. Therefore a large variation in the HVP breakage results would be expected. Indeed Fig. 14 shows the scatter in the Ore A data. This was believed to reflect variation in metal grades. Ore A was also used for HVP pre-concentration tests, in which copper grade variations in the feed particles have been demonstrated (Zuo et al., 2015a). Despite the scatter, the fitting results suggest that the model is robust enough to replicate the complex interaction of different influencing factors on the HVP breakage indices.

Similar to mechanical breakage, there is a relationship between t_{10} and t_n for the HVP breakage. An example of the t_n-t_{10} family of curves is given in Fig. 15. The t_n-t_{10} family of curves will allow the full product size distribution be generated from the t_{10} value predicted by the D_2-model (Eq. (17)). Note that errors are associated with the generalized t_n-t_{10} family of curves. To minimise the errors associated with product size distributions, using the HVP product sizing data to establish a set of ore-specific t_n-t_{10} family of curves for the tested ore sample is preferred.

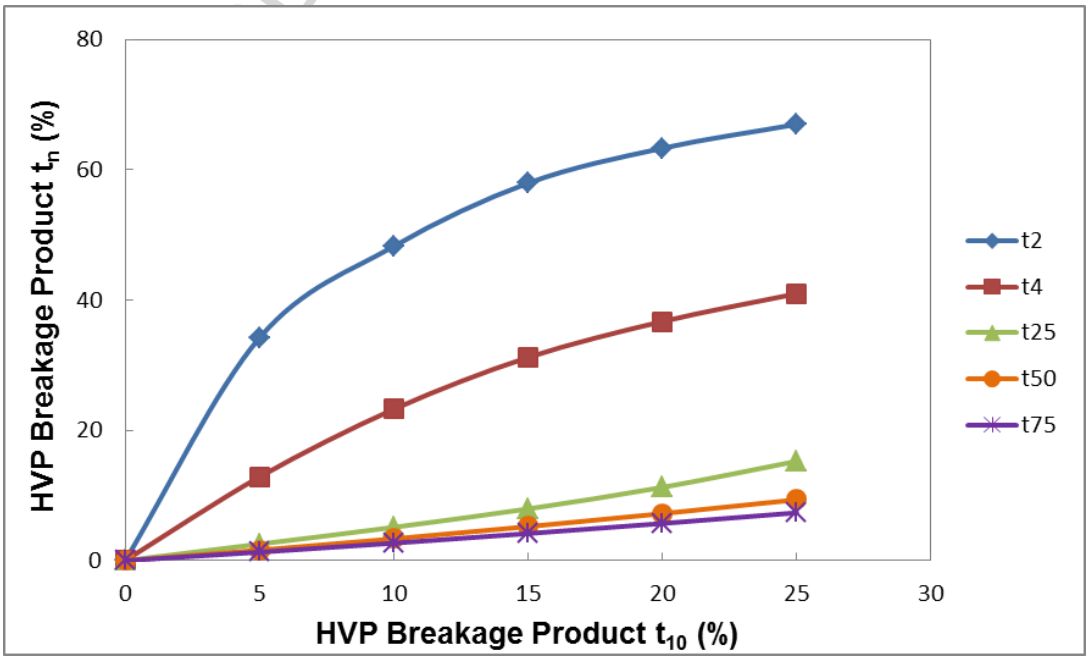

Fig. 15. The t_n-t_{10} family of curves derived from HVP breakage tests on three ore samples (Zuo et al., 2015b)

It was demonstrated that body breakage of particles is often caused by metalliferous grain-induced breakdown, and the index of body breakage probability is closely related to metal grade (Zuo et al., 2015a). It is anticipated that the breakage probability predicted by the D_1-model will closely link with the mass yield of the high grade product when using HVP pre-concentration, thus providing a new opportunity to use the HVP breakage model to predict the recovery of valuable metals. Preliminary results are given in Zuo et al. (2015b). More data are needed for validation and further improvement.

7. Summary and Conclusion

A modelling method that is different to the traditional population balance model for comminution has been reviewed. This modelling approach is based on a mechanistic structure of the energy-size reduction relationship. The JK size-dependent breakage model (Shi and Kojovic, 2007) provides a key mathematical template to rationally link the size reduction as the model output with ore breakage properties and specific energy as the model inputs in a comminution process. This is different to the population balance model, which is based only on the structure of rate-size balance of the size reduction, without directly incorporating the input energy and the material properties that affect the size reduction results in the model structure.

In the energy-size reduction modelling approach, the size reduction output is described by a breakage index, t_{10}, which is a normalised index taking into account the feed particle size (Narayanan and Whiten, 1988). By using the t_n-t_{10} family of curves, the product size distribution can be determined from the single index, t_{10}, alone. The size reduction inputs consist of two categories: material-specific properties and properties related to operational conditions. The material-specific breakage property is described by model parameters *M, p* and *q*, which are determined from breakage characterisation tests on the particular material,

and remain constant during the model fitting process. The breakage characterisation test to determine the material *M, p* and *q* parameters include a single particle impact test using DWT or JKRBT (a rotary breakage tester developed by the JKMRC (Shi et al., 2009), compression bed breakage test using JKFBC, or a piston press test. The material-specific property also includes feed particle size, whose effect on breakage is defined by the characteristic parameter *q*. The second category, the properties related to operational conditions, is described by specific energy.

Five case studies using the energy-size reduction approach for comminution modelling have been reviewed, including a hammer mill for coke feed preparation, a vertical spindle mill for coal PF grinding, a ball mill for batch grinding and continuous operation, HPGR for ore grinding and high voltage pulse disintegration of ores. In these modelling processes, the key was to estimate the specific energy. This involves three common steps described below.

The first step is to estimate power draw or energy consumption. This procedure is machine-dependent, which allows a mechanistic structure be established to link the power draw or energy consumption with machine geometry and operational conditions. In the five cases reviewed, different approaches were taken to model the power draw or energy consumption for different comminution devices. The hammer mill was modelled as a fan consuming power when moving a gas using the law of conservation of energy and Bernoulli's equation. The vertical spindle mill power draw was modelled from physical principles as a product of driving torque multiplied by the angular velocity of the grinding table. The ball mill power draw was calculated by Morrell's power model (Morrell, 1992) that takes account of mill geometry and operational conditions. The HPGR energy consumption was inferred from a piston press test by integrating the resulting force-displacement curves. The high voltage pulse breakage energy was directly calculated from high voltage physics from the machine setting conditions.

The second step is to estimate the specific energy. By definition, specific energy is calculated as energy divided by mass of material for a batch grinding, or power divided by mass flow rate for continuous operation. In some cases such as the hammer mill, the internal circulating load is unknown. The calculated power draw data can be used to estimate the hammer mill content.

It is argued that the mean specific energy calculated in Step 2 cannot be evenly delivered to all sizes of particles. Step 3 is therefore used to estimate the size-specific energy. In the VSM model example, the size specific energy is estimated by an empirical equation with its parameters fitted to the survey data. In the ball mill model, it is described by a selection function with three knot values fitted. This selection function is then used to calculate the size specific energy for all size fractions by a cubic spline function.

There are a number of advantages in using the energy-size reduction approach for comminution modelling, attributable to the decoupled material property and the operational conditions in the model. As the material breakage properties are measured, and the characteristic parameters are explicitly incorporated in the energy-size reduction model, it is possible to run simulations for ore/coal changes, including the feed size variation, on comminution performance. Another advantage is that, because the size-specific energy in the model is mechanistically modelled as a function of machine geometry and operating condition, it is possible to use the model to optimise a comminution machine or a circuit by varying the geometry or the operating conditions.

It is understood that the objective of comminution is not only for size reduction, but also for valuable mineral liberation. Since the liberation must be associated with particle size reduction, the energy-size reduction approach may be used as a basis for liberation. This requires further work, in which the JK size-dependent breakage model may play a role in liberation modelling.

Acknowledgement

Financial support of the JKMRC projects reviewed in this article was provided by the following organisations: AMIRA P9N Program for the development of the JK size-dependent breakage model, Anglo American, Barrick Gold, BHP Billiton, Rio Tinto, Teck and JKTech in the JKRBT and size dependent breakage model validation project, ACARP C8057 Project for hammer mill model, the Australian Government Department of Resources, Energy and Tourism in the Asia-Pacific Partnership on Clean Development and Climate program (APP) for the vertical spindle mill model, AMIRA P9P Program for the specific energy based ball mill model, Newcrest Mining for the high voltage pulse breakage model. The author has had the pleasure of working with his JKMRC colleagues in developing the JK size-dependent breakage model and applying it for the mineral and coal industries. In particular, the contributions made by the following JKMRC colleagues are gratefully acknowledged: Dr Toni Kojovic in the JKRBT, the JK size-dependent breakage model, the hammer mill model and the vertical spindle mill models; Professor William Whiten for the t_n-t_{10} family of curves that were utilised in all the JKMRC models reviewed in this paper and the classification equation used in the specific energy based ball mill model; Professor Alban Lynch in power station grinding work; Professor Emmy Manlapig in the JKRBT and the high voltage pulse research projects; Dr Stephen Morrell for the power model used in the specific energy based ball mill model; Professor Tim Napier–Munn in statistical analysis of the data; Dr Rob Morrison in the incremental breakage; Professor Malcolm Powell in comminution modelling; Dr Matthew Brennan in the vertical spindle mill models, Dr Weiguo Xie in the specific energy based ball mill model, and many postgraduate students whose work has been reviewed in the papers as co-authors. The present author enjoys working with a number of research collaborators involved in the projects reviewed in this series of papers: Professor Yaqun He and his team in China University of Mining and Technology in Xuzhou, Dr Alexander Weh and Dr Klaas van der Wielen of SELFRAG AG in Switzerland, Mr Philip Bennett of ALS

Coal in Brisbane, Dr Terry Dixon of Tarong Power Station in Queensland, Dr Tom Callcott of Callcott Consulting Pty. Ltd and Professor Joan Esterle of CSIRO Exploration and Mining (now at the School of Earth Sciences of the University of Queensland). The author sincerely appreciates the review and the valuable comments on the three review articles in the series by Professor Tim Napier-Munn.

References

Austin, L.G., 1971-72. A review introduction to the mathematical description of grinding as a rate process. Powder Technology, 5: 1-17.

Austin, L.G., Klimpel, R.R., Luckie, P.T., 1984. Process engineering of size reduction: ball milling. The Pennsylvania State University, SME.

Austin, L.G., Luckie, P.T. and Shoji, K., 1982. An analysis of ball-and-race milling Part II: The Badcock E1.7 mill. Powder Technology, 33, 113-125.

Banini, G.A., 2000. An integrated description of rock breakage in comminution machines. Ph.D. Thesis, University of Queensland (JKMRC), Australia.

Callcott T.G. A study of size reduction mechanism of swing hammer mills. J. Inst. Fuel, 33, 1960, 529–39

Carvalho, R.M. and Tavares, L.M., 2013. Predicting the effect of operating and design variables on breakage rates using the mechanistic ball mill model. Minerals Engineering, 43-44, 91-101.

Davaanyam, Z., 2015. Piston press test procedures for predicting energy–size reduction of high pressure grinding rolls. Ph.D. Thesis, The University of British Columbia, Canada.

Davaanyam, Z., Klein, B. and Nadolski, S., 2015. Using piston press tests for determining optimal energy input for an HPGR operation. SAG 2015 Conference, UBC/CIM, Vancouver, Canada, Paper 23.

Djordjevic, N., Shi, F. and Morrison, R.D., 2003. Applying discrete element modelling to vertical and horizontal shaft impact crushers. Minerals Engineering, 16, 983-991.

He, Y., Zuo, W., Duan, C., Zhou, N. and Wang, S., 2011. CUMT plant work and data analysis. In F. Shi (Ed.): APP Final Report – Efficiency Improvement in Coal Fired Utilities, Chapter 2.

Herbst, J.A. and Fuerstenau, D.W., 1973. Mathematical simulation of dry ball milling using specific power information. Transaction SME-AIME, 254, 343–348.

Herbst, J.A. and Fuerstenau, D.W., 1980. Scale-up procedure for continuous grinding mill design using population balance models. International Journal of Mineral Processing, 7, 1–31.

Herbst, J.A. and Mika, T.S., 1970. Mathematical simulation of tumbling mill grinding: an improved method. Rudy, 18(3/4): 70-75.

Hukki, R.T., 1962. Proposal for a solomnic settlement between the theories of von Rittinger, Kick and Bond. Transactions of the AIME 223, 403– 408.

Kelsall, D.F. and Reid, K.J., 1965. The derivation of a mathematical model for breakage in a small, continuous, wet, ball mill. American Institute of Chemical Engineers – Institution of Chemical Engineers Symposium, Series No. 4, 14-20.

King, R.P. and Bourgeois, F., 1993. Measurement of fracture energy during single-particle breakage. Minerals Engineering, 6, 353–367.

Kojovic, T., Shi, F. and Brennan M., 2015. Modelling of vertical spindle mills Part 2: Integrated models for E-mill, MPS and CKP mills. Fuel, 143, 602-611.

Man, Y.T., 2001. Model-based procedure for scale-up of wet, overflow ball mills, Part 1: Outline of the methodology. Minerals Engineering, 14 (10), 1237-1246.

Morrell, S., 1992. Prediction of grinding mill power. Transactions of the Institution of Mining and Metallurgy, Section C, 101, C25-32.

Morrell, S., 2004. An alternative energy–size relationship to that proposed by Bond for the design and optimisation of grinding circuits. International Journal of Mineral Processing, 74, 133-141.

Morrell, S., Lim, W., Shi, F. and Tondo, L., 1997a. Modelling of the HPGR crusher. SME Annual Conference (Kawatra Ed.), Denver, USA: Chapter 17, 117-126.

Morrell, S., Shi, F. and Tondo, L., 1997b. Modelling and scale-up of high pressure grinding rolls. The 20th International Mineral Processing Congress, Vol. 2: 129-140.

Morrell, S., Sterns, U.J. and Weller, K.R., 1993. The application of population balance models to very fine grinding in tower mills. The 18th International Mineral Processing Congress, Sydney, 61-66.

Napier-Munn, T.J., Morrell, S., Morrison, R.D., and Kojovic, T., 1996. Mineral comminution circuits: their operation and optimisation. ISBN 0 646 28861 x. Julius Kruttschnitt Mineral Research Centre.

Narayanan, S.S., and Whiten, W.J., 1988. Determination of comminution characteristics from single particle breakage tests and its application to ball mill scale-up. Trans. Inst. Miner. Metall. 97, C115-C124.

Özer, C., Shi, F. and Whiten, W., 2009. Improving the efficiency of fine coal grinding circuits – Tarong power station site work. ACARP C15079 Final Report. <http://www.acarp.com.au/abstracts.aspx?repId=C15079>

Parker, T., Shi, F., Evans C. and Powell, P., 2015. The effects of electrical comminution on the mineral liberation and surface chemistry of a porphyry copper ore. Minerals Engineering, 82, 101-106

Rumpf, H., 1973. Physical aspects of comminution and a new formulation of a Law of Comminution. Powder Technology 7, 145– 159.

Sato, K., Meguri, N., Shoji, K., Kanemoto, H., Hasegawa, T. and Maruyama, T., 1996. Breakage of coals in ring-roller mills Part 1: The breakage properties of various coals and simulation model to predict steady-state mill performance. Powder Technology, 86(3), 275-283.

Shi, F., 2002. Development of a power draw model for estimation of the dynamic recirculating load of swing hammer mills with internal classifiers. Trans. Instn Min. Metall. (Sect. C: Mineral Process. Extr. Mrtall.), 111-119/Proc. Australas. Inst. Min. Metall., 307, September-December 2002.

Shi, F., 2016. A review of the applications of the JK size-dependent breakage model Part 1: Ore and coal breakage characterisations. International Journal of Mineral Processing, 155, 118-129.

Shi, F., Kojovic, T. and Brennan M., 2015a. Modelling of vertical spindle mills Part 1: Sub-models for comminution and classification. Fuel, 143, 595-601.

Shi, F., Kojovic, T., Esterle, J. and David, D., 2003. An energy-based model for swing hammer mills. International Journal of Mineral Processing, 71, 147-166.

Shi, F., Kojovic, T., Larbi-Bram, S. and Manlapig, E., 2009. Development of a rapid particle breakage characterization device – the JKRBT. Minerals Engineering, 22, 602-612.

Shi, F. and Napier-Munn, T.J., 2002. Effects of slurry rheology on industrial grinding performance. International Journal of Mineral Processing, 65/3-4, 125-140.

Shi, F. and Zuo, W., 2014. Coal breakage characterisation - Part 1: Breakage testing with the JKFBC. Fuel, 117, 1148-1155.

Shi, F., Zuo, W. and Manlapig, E., 2015b. Pre-concentration of copper ores by high voltage pulses, Part 2: Opportunities and challenges. Minerals Engineering, 79, 315-323.

Shoji, K., Meguri, N., Sato, K., Kanemoto, H., Hasegawa, T. and Maruyama, T., 1998. Breakage of coals in ring-roller mills Part 2: An unsteady-state simulation model. Powder Technology, 99(1), 46-52.

Sligar, N.J. 1975. Estimation of crushing and classification functions for and mathematical simulation of a medium speed roll/table mill. PhD Thesis, University of Newcastle.

Sproull, W. T., 1970. Air pollution and its control. Exposition Press, Jericho, New York.

Tavares, L.M. and King, R.P., 1998. Single-particle fracture under impact loading. International Journal of Mineral Processing, 54, 1-28.

van der Wielen, K.P., Pascoe, R., Weh, A., Wall, F., Rollinson, G., 2013. The influence of equipment settings and rock properties on high voltage breakage. Minerals Engineering, 46–47, 100-111.

Vogel, L. and Peukert, W., 2003a. Breakage behaviour of different materials – construction of a mastercurve for the breakage probability. Powder Technology. 129, 101-110.

Wang, E., Shi, F. and Manlapig, E., 2011. Pre-weakening of mineral ores by high voltage pulses. Minerals Engineering, 24, 455-462.

Wang, E., Shi, F. and Manlapig, E., 2012. Mineral liberation by high voltage pulses and conventional comminution with same specific energy levels. Minerals Engineering, 27-28, 28-36.

Weichert, R., 1988. Correlation between probability of breakage and fragment size distribution of mineral particles. International Journal of Mineral Processing, 22, 1-8.

Whiten, W.J., 1974. A matrix theory of comminution machines. Chemical Engineering Science, 29, 31–34.

Zuo, W., Shi, F. and Manlapig, E., 2015a. Pre-concentration of copper ores by high voltage pulses, Part 1: Principle and major findings. Minerals Engineering, 79, 306-314.

Zuo, W., Shi, F. and Manlapig, E., 2015b. Modelling of high voltage pulse breakage of ores. Minerals Engineering, 83, 168-174.

Zuo, W., Shi, F., van der Wielen, K. and Weh, A., 2015. Ore particle breakage behaviour in a pilot scale high voltage pulse machine. Minerals Engineering, 84, 64-73.

Part 3 Research Highlights

- Using the energy-size reduction relationship for comminution equipment modelling
- Five comminution models based on the energy-size reduction relationship reviewed
- The JK size-dependent breakage model provides a key mathematical template.
- Capability to simulate the effects of changes in ore/coal and machine conditions